Chirality-Dependent Hall Effect and Antisymmetric Magnetoresistance in a Magnetic Weyl Semimetal

Bingyan Jiang, Lujunyu Wang, Ran Bi, Juewen Fan, and Jiaji Zhao
State Key Laboratory for Artificial Microstructure and Mesoscopic Physics, Frontiers Science Center for Nano-optoelectronics, Peking University, Beijing 100871, China

Dapeng Yu
Shenzhen Institute for Quantum Science and Engineering, Southern University of Science and Technology, Shenzhen 518055, China

Zhilin Li*
Beijing National Laboratory for Condensed Matter Physics, Institute of Physics, Chinese Academy of Sciences, Beijing 100190, China

Xiaosong Wu†
State Key Laboratory for Artificial Microstructure and Mesoscopic Physics, Frontiers Science Center for Nano-optoelectronics, Peking University, Beijing 100871, China; Collaborative Innovation Center of Quantum Matter, Beijing 100871, China; and Shenzhen Institute for Quantum Science and Engineering, Southern University of Science and Technology, Shenzhen 518055, China

(Received 7 January 2021; accepted 11 May 2021; published 8 June 2021)

Weyl semimetals host a variety of exotic effects that have no counterpart in conventional materials, such as the chiral anomaly and magnetic monopole in momentum space. These effects give rise to unusual transport properties, including a negative magnetoresistance and a planar Hall effect, etc. Here, we report a new type of Hall and magnetoresistance effect in a magnetic Weyl semimetal. Unlike antisymmetric (with respect to *either* magnetic field *or* magnetization) Hall and symmetric magnetoresistance in conventional materials, the discovered magnetoresistance and Hall effect are antisymmetric in *both* magnetic field *and* magnetization. We show that the Berry curvature, the tilt of the Weyl node, and the chiral anomaly synergically produce these phenomena. Our results reveal a unique property of Weyl semimetals with broken time reversal symmetry.

DOI: 10.1103/PhysRevLett.126.236601

Electrical resistivity is one of the most basic properties of condensed matter and hence is extensively used as a characterization tool. It can be represented by a second-rank tensor ρ_{ij} in linear response. Under a magnetic field B, the Onsager reciprocity relations require $\rho_{ij}(B) = \rho_{ji}(-B)$ [1]. Consequently, the diagonal elements $\rho_{ii}(B)$, magnetoresistance (MR), is symmetric in B. The off-diagonal elements ($i \neq j$) can be divided into two components based on the symmetry under exchange of two coordinates, i.e., the symmetric one $\rho_{ij} = \rho_{ji}$ and the antisymmetric one $\rho_{ij} = -\rho_{ji}$. Applying the Onsager reciprocity relations to them yields $\rho_{ij}(B) = \rho_{ij}(-B)$ for the symmetric one, and $\rho_{ij}(B) = -\rho_{ij}(-B)$ for the antisymmetric one. The former is anisotropic magnetoresistance, although it is sometimes called the planar Hall effect [2]. It takes place in magnetic materials and was recently found in Weyl semimetals due to the chiral anomaly [2–6]. The latter is the Hall effect. In the case of the magnetic field being the time reversal symmetry (TRS) breaking field, deflection of carriers by the Lorentz force gives rise to the ordinary Hall effect (OHE). In the case of the exchange field being the TRS breaking field, the anomalous Hall effect (AHE) arises, which is antisymmetric in magnetization M, $\rho_{ij}(M) = -\rho_{ij}(-M)$ [7]. AHE is the result of Berry curvature in the band structure, which acts on carriers as a fictitious magnetic field in momentum space [8]. This difference in symmetry is routinely utilized to separate contributions from MR and Hall resistance.

When there are more than one TRS breaking fields, the Onsager reciprocity relations still hold provided that one reverses all of these fields [9]. Consequently, the common symmetry of the resistivity tensor elements will be altered. However, this phenomenon has rarely been observed [10]. Recently, there have been predictions on how Weyl semimetals may realize a resistivity of such symmetries [11–19]. Cortijo proposed as a candidate TRS breaking Weyl semimetals with band-bending terms [11]. Others suggested that the tilted Weyl semimetals can introduce this effect, too [12–18]. Whereas most studies were focused on

band structure anisotropies, Xiao *et al.* studied the effect of intrascattering of Bloch electrons augmented by the Berry curvature, magnetic moment, and shift vector [19]. They found that the unusual TRS breaking field symmetry may appear in many systems, as the crystal symmetry requirement is less stringent than the widely observed AHE.

In this work, we report experimental observation of a resistivity tensor with aforementioned symmetries in a magnetic Weyl semimetal $Co_3Sn_2S_2$. A prominent Hall effect antisymmetric in both B and M is observed. The field angular dependence indicates that this effect is dependent on the out-of-plane magnetization and the in-plane field, which normally does not contribute to the Hall effect. In addition, the MR is also antisymmetric in magnetization and field. These observations can be understood in terms of tilted Weyl nodes in combination with the chirality, chiral anomaly, and broken time reversal symmetry.

$Co_3Sn_2S_2$ single crystals were grown by the chemical vapor transport method using pre-synthesized polycrystalline ingot as the starting material and elemental iodine as the transport agent, in a temperature gradient of about 850 to 830 °C. The crystal structure was confirmed by the x-ray diffraction method. The crystals have smooth and shiny surfaces and usually hexagonal facets in size of 1–2 mm. They were sanded and polished to a thickness of 60 μm for electrical measurements. Electrical contacts were made by silver paste. Four-probe electrical measurements were carried out using a low frequency lock-in method. The current was along the x axis, as indicated in the inset of Fig. 1(a). A typical current of 1 mA was used. The dependence of the resistance on the amplitude of current up to 5 mA was checked to make sure that there was no nonlinearity, nor appreciable heating. Samples were

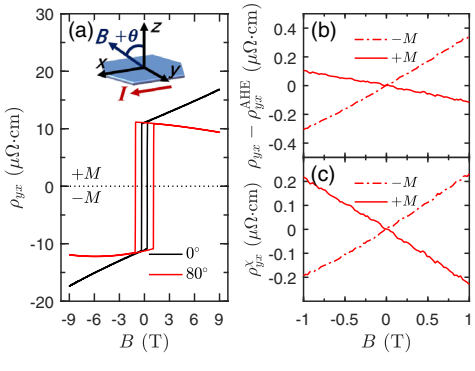

FIG. 1. Chirality-dependent in-plane Hall effect at $T = 20$ K. (a) Hall resistivity for magnetic field at $\theta = 0°$ and 80°. The inset depicts the direction of current and the magnetic field. (b) Hall resistivity below B_c after subtracting AHE. The difference between these two lines is inconsistent with OHE, implying an extra Hall resistivity. (c) Hall resistivity after subtracting OHE and AHE, denoted as ρ_{yx}^{χ}. It is linear and antisymmetric in the magnetic field and changes its sign when the magnetization reverses polarity. The antisymmetry also suggests that symmetric magnetoresistance due to contact misalignment is negligible.

mounted on a motorized rotator stage with a resolution better than 0.02°. Two samples were successfully measured and show nearly identical behaviors. Data for sample B04 are presented in the main text. Data for sample B01 can be found in Supplemental Material [20].

$Co_3Sn_2S_2$ is the first experimentally confirmed magnetic Weyl semimetal and thereafter has attracted significant attention [21–34]. Its lattice has a rhombohedral structure belonging to the space group $R\bar{3}m$. Owing to the threefold rotational symmetry along the z axis, it features three pairs of Weyl nodes in the bulk and the nontrivial surface states, Fermi arcs, on the surface [25,26]. The separation between two Weyl nodes in a pair is relatively large, giving rise to a strong anomalous Hall effect [21,22,35]. Our samples exhibit characteristics of $Co_3Sn_2S_2$ consistent with previous reports, shown in Supplemental Material [20]. The temperature dependent resistivity indicates a Curie temperature of 175 K, below which a large AHE appears. The maximum Hall conductivity is about 1200 S cm^{-1}. When the magnetic field is along the z axis ($B_\perp$), the Hall effect consists of both OHE and AHE, $\rho_{yx} = \rho_{yx}^{\mathrm{OHE}} + \rho_{yx}^{\mathrm{AHE}}$, seen in Fig. 1(a). Following the general treatment for $Co_3Sn_2S_2$ [21,30,32,34,36], the AHE is taken as a constant, $\rho_{yx}^{\mathrm{AHE}} = \rho_{yx}(B = 0)$, while the field dependence of ρ_{yx} above the coercive field B_c is regarded as the OHE component. A constant AHE is justified by the fact that the magnetization of $Co_3Sn_2S_2$ saturates above B_c at temperatures well below the Curie temperature [22,23,36,37]. In contrast to some reports, in which ρ_{yx}^{OHE} is nonlinear in B [21,34], the OHE of our samples is linear in B, that is, $\rho_{yx}^{\mathrm{OHE}} = R_0 B$, where $R_0 = 0.63\ \mu\Omega\,\mathrm{cm/T}$ is the OHE coefficient. A single band conduction suggested by the linearity makes our analysis more straightforward.

As expected, the OHE is antisymmetric in B and the AHE is antisymmetric in M. However, when the magnetic field is tilted by θ degrees away from the z axis toward the x axis, ρ_{yx} obviously deviates from a pure antisymmetric behavior. For instance, at $\theta = 80°$, the overall slope of $\rho_{yx}(B)$ is negative for positive M, while it is positive for negative M. This difference in slope is illustrated better in Fig. 1(b) where ρ', defined as $\rho_{yx}(B) - \rho_{yx}^{\mathrm{AHE}}$, is plotted below B_c. If one further removes the OHE component by $\rho' - R_0 B_\perp$, where $R_0 = 0.63\,\mu\Omega$ cm/T and $B_\perp = B\cos\theta$, one will notice that not only the remaining Hall resistivity is linear and antisymmetric in B, the slope simply reverses sign while maintaining its amplitude when M is reversed. In other words, this extra Hall, denoted as ρ_{yx}^{χ}, is antisymmetric in both B and M,

$$\rho_{yx}^{\chi}(M,B) = -\rho_{yx}^{\chi}(M,-B) = -\rho_{yx}^{\chi}(-M,B) = \rho_{yx}^{\chi}(-M,-B). \tag{1}$$

Since it emerges when B is tilted away from the z axis, it is reasonable to assume that it depends on the in-plane field

$B_\parallel$. Moreover, due to the strong magnetic anisotropy in $Co_3Sn_2S_2$, M aligns closely to the z axis [21,36,37]. Considering the observed linear field dependence, we tentatively propose $\rho_{yx}^{\chi} \propto M_z B_\parallel$.

The Hall nature (antisymmetric in B) of ρ_{yx}^{χ} is apparent below B_c, where M_z remains unchanged. However, above B_c, where M_z switches polarity, $\rho_{yx}^{\chi}(M_z, B_\parallel) = \rho_{yx}^{\chi}(-M_z, -B_\parallel)$ appears B symmetric, disguising its Hall nature. To obtain $\rho_{yx}^{\chi}(M_z, B_\parallel)$ in the whole field range with the same M_z, we measure the Hall resistance at $\pm\theta$. Such geometries allow one to switch the polarity of the parallel field without altering M_z. It is obvious that $\rho_{yx}^{\chi} = [\rho'(\theta) - \rho'(-\theta)]/2$ and $\rho_{yx}^{\mathrm{OHE}} = [\rho'(\theta) + \rho'(-\theta)]/2$. We obtain ρ'_{yx} by $\rho'_{yx}(\theta) = \rho_{yx}(\theta) - \rho_{yx}^{\mathrm{AHE}}(\theta)$, where $\rho_{yx}^{\mathrm{AHE}}(\theta)$ takes a value of the zero field AHE. Although the actual $\rho_{yx}^{\mathrm{AHE}}(\theta)$ is likely dependent on B when the field is not along the z axis, the estimation of ρ_{yx}^{χ} will not be affected, because $\rho_{yx}^{\mathrm{AHE}}(\theta) = \rho_{yx}^{\mathrm{AHE}}(-\theta)$ and they are canceled by antisymmetrizing. This field dependence goes into ρ_{yx}^{OHE}, which will be discussed later. Moreover, the antisymmetrizing method is effective in removing magnetoresistance component resulting from inevitable contact misalignment, as the magnetoresistance at $\pm\theta$ are equal when the field is in the xz plane, seeing the analysis of ρ_{xx}. Figure 2 illustrates the two Hall components extracted for $\theta = \pm 50°$ (data for other angles can be found in Supplemental Material [20]). Both show a linear dependence at low fields. The angular dependence of the

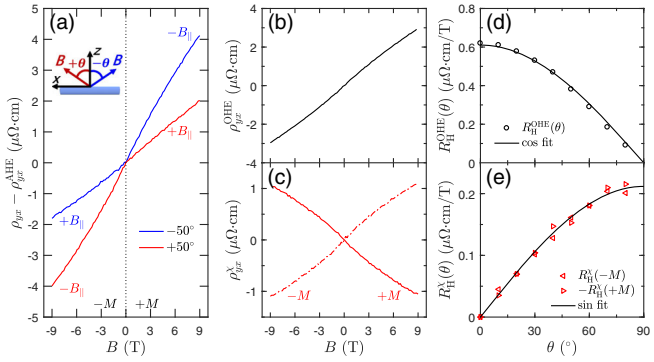

FIG. 2. Extraction of the chirality-dependent Hall effect at $T = 20$ K for magnetic field in the xz plane. (a) Hall resistivity after subtracting AHE at $\theta = \pm 50°$. To remove overlapped data between $\pm B_c$, the data between -9 to 0 T are plotted for sweeping up, while the data between 0 to 9 T are plotted for sweeping down. The inset depicts the magnetic field direction. When the angle is changed from positive to negative ($+\theta$ to $-\theta$), the in-plane magnetic field is reversed ($+B_\parallel$ to $-B_\parallel$) while the magnetization keeps its sign, resulting in ρ_{yx}^{χ} in the opposite field without altering OHE and AHE. (b),(c) The extracted OHE and ρ_{yx}^{χ}, respectively. Both show a linear dependence at low fields. (d) Angular dependence of the Hall coefficient of OHE. The solid line is a fit to $\cos\theta$. (e) Angular dependence of the Hall coefficient of ρ_{yx}^{χ}. The solid line is a fit to $\sin\theta$.

Hall coefficient follows a cosine function, consistent with $\rho_{yx}^{\mathrm{OHE}} = R_0 B_\perp$, which verifies our method of decomposing two Hall components. In addition, the angular dependence of the low field slope of ρ_{yx}^{χ} satisfies a sine function, supporting the assumption of $\rho_{yx}^{\chi} \propto B_\parallel$. This unconventional Hall effect is significant, as its amplitude, 0.21 $\mu\Omega\,\mathrm{cm/T}$, amounts to one-third of the OHE.

Both ρ_{yx}^{OHE} and ρ_{yx}^{χ} deviate from linearity at high fields. To understand it, one needs to note that a large in-plane field can slightly tilt M away from the z axis, despite the strong magnetic anisotropy in $Co_3Sn_2S_2$ [21,36,37]. The resultant reduction of M_z leads to a decrease of ρ_{yx}^{AHE}, which was, however, taken as a constant when extracting ρ_{yx}^{OHE}. Consequently, this procedure underestimates ρ_{yx}^{OHE}, which explains the suppression of ρ_{yx}^{OHE} at high fields. If ρ_{yx}^{χ} is indeed proportional to M_z as we assume, similar depression of ρ_{yx}^{χ} would be anticipated. This is exactly what we observe in experiment, which supports that ρ_{yx}^{χ} depends on M_z. The same set of measurements were carried out when the magnetic field was tilted in the yz plane (see Supplemental Material [20]). In stark contrast, $\rho_{yx}^{\chi} \approx 0$. Therefore, the expression for ρ_{yx}^{χ} can be narrowed down to $\rho_{yx}^{\chi} \propto M_z B_x$.

We now turn to the diagonal element of the resistivity tensor, ρ_{xx}. Under a perpendicular field, ρ_{xx} exhibits a small positive MR. A jump appears at B_c, likely due to the AHE contribution introduced by contact misalignment. It is manually offset in the following data analysis. When the field is tilted by $\pm 70°$ toward the y axis, ρ_{xx} displays a striking difference between two tilt angles, as seen in Fig. 3. For $\theta = -70°$, MR is positive, while it turns negative for $\theta = 70°$. What is even more intriguing is that MR displays a Hall-like behavior (B antisymmetric) at low fields before M is reversed at B_c. The slope reverses sign when M_z is reversed, just like ρ_{yx}^{χ}. Although contact misalignment may introduce a component of ρ_{yx}, the Hall-like behavior of ρ_{xx} cannot come from ρ_{yx}^{χ}, as ρ_{yx}^{χ} only appears when the field in the xz plane and is approximately zero when the field is in the yz plane. Thus, we validate a MR that is antisymmetric in both $B_\parallel$ and M_z, $\rho_{xx}^{\chi} \propto M_z B_\parallel$. Above B_c, where M_z switches sign, ρ_{xx}^{χ} looks symmetric in B, making its Hall-like field dependence less obvious. The same procedure used for ρ_{yx}^{χ} is performed to extract ρ_{xx}^{χ} and the conventional MR symmetric in B for the whole field range, i.e., $\rho_{xx}^{\chi} = [\rho_{xx}(\theta) - \rho_{xx}(-\theta)]/2$ and $\rho_{xx}^{\mathrm{sym}} = [\rho_{xx}(\theta) + \rho_{xx}(-\theta)]/2$. Again, any contribution from OHE and AHE due to contact misalignment will be removed from ρ_{xx}^{χ} by antisymmetrizing. The conventional MR traces as a function of the perpendicular field $B_\perp$ at different θ collapse onto a single one with a B^2 dependence, which again verifies our method and suggests that this MR is determined by $B_\perp$. ρ_{xx}^{χ} looks nearly identical to ρ_{yx}^{χ}. A good scaling of data at different θ is achieved when it is plotted against $B_\parallel$, as shown in

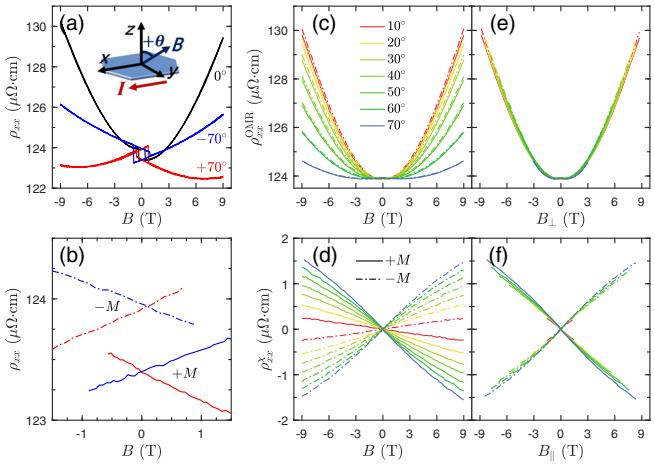

FIG. 3. Antisymmetric linear MR at $T = 20$ K for magnetic field in the yz plane. (a) MR at $\theta = 0°$ and $\pm 70°$. The jump at B_c is most likely induced by AHE due to non-ideal voltage contacts. (b) Close-up of MR below the coercive field. Solid and dashed lines represent the positive and negative magnetization, respectively. The slope depends on the polarity of magnetization. (c),(d) Extracted ordinary and chirality-dependent MR, respectively. (e) Ordinary MR as a function of the perpendicular magnetic field $B_\perp$. (f) Chirality-dependent MR as a function of the in-plane magnetic field $B_\parallel$.

Fig. 3(f). Similar to ρ^{χ}_{yx}, a suppression at high fields can be explained by tilting of the magnetization, indicating $\rho^{\chi}_{xx} \propto M_z$. When the field is tilted in the xz plane, ρ^{χ}_{xx} is essentially zero (seen in Supplemental Material [20]). On the basis of these results, we conclude that $\rho^{\chi}_{xx} \propto M_z B_y$.

Having established the field and magnetization dependence of ρ^{χ}_{yx} and ρ^{χ}_{xx}, we map out their field angular dependence by measuring the Hall resistance and MR as a function of the tilt angle at $B = 9$ T, shown in Fig. 4. ρ_{yx} exhibits a clear asymmetry when B is rotated in the xz plane, while it is rather symmetric when B is in the yz plane. After extraction of ρ^{χ}_{yx}, the dependence of its sign on B_x and M_z is well illustrated in the polar plot, in agreement with Eq. (1). In contrast, ρ_{xx} displays the opposite behavior. It is symmetric when B is rotated in the xz plane, while it becomes asymmetric when B is in the yz plane. Consequently, ρ^{χ}_{xx} emerges when the field is in the yz plane. Nevertheless, the similarity between ρ^{χ}_{yx} and ρ^{χ}_{xx} strongly suggests the same origin. It is worth reiterating that these effects are truly B antisymmetric. The reason that the angular dependence of these two contributions shows a π periodicity (B symmetric), is because M switches polarity with B above the coercive field. Experimentally, the B-antisymmetric behavior due to these effects cannot be directly observed in nonmagnetic materials or soft magnets, but only in magnets with spontaneous magnetization.

In Weyl semimetals subject to parallel electric and magnetic fields, the chiral anomaly arises, leading to a B^2 negative magnetoresistance [38,39] and a planar Hall effect [2–6]. In condensed matter systems, the Weyl node is allowed to tilt, breaking the Lorentz invariance. In fact, tilting is much more likely than not in real materials. In TRS breaking Weyl semimetals, where the inversion symmetry is present, Weyl cones with different chiralities tilt to the opposite direction, producing currents that depend antisymmetrically and linearly on magnetic field [12–17]. The detailed explanation can be found in Supplemental Material [20], while for a more thorough picture and derivation, we refer readers to those theoretical works [12–17]. Three additional currents driven by the electric field $\boldsymbol{E}$ are introduced. They stem from the anomalous velocity $(\boldsymbol{v_k} \cdot \boldsymbol{\Omega_k})\boldsymbol{B}$ due to the Berry curvature, the chiral chemical potential $(\boldsymbol{B} \cdot \boldsymbol{E})(\boldsymbol{v_k} \cdot \boldsymbol{\Omega_k})$ generated by the chiral anomaly and the Berry curvature correction to the phase space volume $[1 + (e/\hbar)(\boldsymbol{B} \cdot \boldsymbol{\Omega_k})]^{-1}$. Here, $\boldsymbol{v_k}$ and $\boldsymbol{\Omega_k}$ are the group velocity and the Berry curvature, respectively. The first current is directed along the magnetic field, $\boldsymbol{j} \propto (\boldsymbol{E} \cdot \hat{\boldsymbol{R}})\boldsymbol{B}$. The second one is along the direction of the tilt axis $\hat{\boldsymbol{R}}$, $\boldsymbol{j} \propto (\boldsymbol{E} \cdot \boldsymbol{B})\hat{\boldsymbol{R}}$. The third one can contribute to a current along the electric field, $\boldsymbol{j} \propto (\boldsymbol{B} \cdot \hat{\boldsymbol{R}})\boldsymbol{E}$ [16].

In a general configuration of $(\boldsymbol{E}, \boldsymbol{B}, \hat{\boldsymbol{R}})$, the first two currents can be at an arbitrary angle with the electric field, contributing to both ρ^{χ}_{xx} and ρ^{χ}_{yx}. For simplicity, let us consider a special case in which $\boldsymbol{B}$, $\boldsymbol{E}$, and $\hat{\boldsymbol{R}}$ are coplanar and $\boldsymbol{E} \perp \hat{\boldsymbol{R}}$. When $\boldsymbol{B}$ is perpendicular to $\hat{\boldsymbol{R}}$, a transverse current of $\boldsymbol{j} \propto (\boldsymbol{E} \cdot \boldsymbol{B})\hat{\boldsymbol{R}}$ appears, giving rise to ρ^{χ}_{yx}, while the longitudinal current is zero. When $\boldsymbol{B}$ is parallel to $\hat{\boldsymbol{R}}$, a longitudinal current of $\boldsymbol{j} \propto (\boldsymbol{B} \cdot \hat{\boldsymbol{R}})\boldsymbol{E}$ appears, giving rise to ρ^{χ}_{xx}, while the transverse current is zero. The currents reverse sign when two Weyl nodes with opposite chirality flip their chiralities, which happens when the magnetization is reversed [40]. Although these theoretical studies predict corrections to the conductivity $\Delta\sigma$, the corresponding corrections to the resistivity $\Delta\rho$ are proportional to $\Delta\sigma$ when $\rho_{xx} \gg \rho_{yx}$, i.e., $\Delta\sigma_{yx} = (\Delta\rho_{yx}/\rho^2_{xx} + \rho^2_{yx}) \approx \Delta\rho_{yx}/\rho^2_{xx}$ and $\Delta\sigma_{xx} = (\Delta\rho_{xx}/\rho^2_{xx} + \rho^2_{yx}) \approx \Delta\rho_{xx}/\rho^2_{xx}$. In $Co_3Sn_2S_2$, $\rho_{xx} \approx 100\ \mu\Omega\,\mathrm{cm} \gg \rho_{yx} \approx 10\ \mu\Omega\,\mathrm{cm}$. Therefore, our field dependent resistivity tensor is in excellent agreement with above predictions, implying that the tilt axis is along the y axis. However, there would be three tilt axes in $Co_3Sn_2S_2$ linked by the C_{3z} symmetry. Their contributions compete. To fully understand our experiment, calculations of the chiral current for general magnetic field directions based on the actual band structure of $Co_3Sn_2S_2$ is required. The picture of the chiral current is further corroborated by measurements with the current along the y axis. In the configuration of $\boldsymbol{E} \| \boldsymbol{y} \| \hat{\boldsymbol{R}}$, it has been observed that ρ^{χ}_{xy} occurs when $\boldsymbol{B} \| \boldsymbol{x}$, corresponding to $\boldsymbol{j} \propto (\boldsymbol{E} \cdot \hat{\boldsymbol{R}})\boldsymbol{B}$, while ρ^{χ}_{yy} emerges when $\boldsymbol{B} \| \boldsymbol{y}$, where all three currents may contribute [41].

In summary, we discover a chirality-dependent Hall effect and magnetoresistance that are antisymmetric in

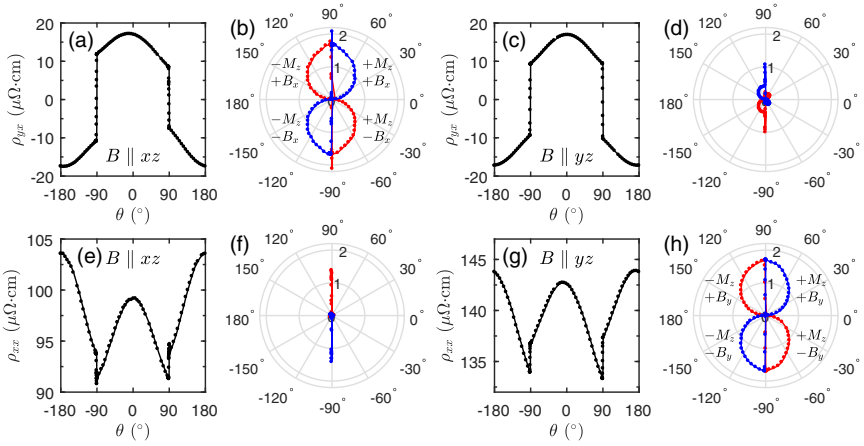

FIG. 4. Angular dependence of the chirality-dependent resistivity tensor for $B = 9$ T in the xz and yz planes. (a) ρ_{yx} with field in the xz plane. The discontinuities are caused by the sudden flip of the magnetization across the parallel position ($\theta = \pm 90°$). The difference between two discontinuities is a manifest of ρ^{χ}_{yx}. (b) ρ^{χ}_{yx} extracted from (a) in polar coordinates. Red and blue represent positive and negative values, respectively. The polarity of B_x and M_z is labeled for four quadrants, highlighting the antisymmetric relations indicated by Eq. (1). (c) ρ_{xy} with field in the yz plane. No substantial asymmetry observed. (d) ρ^{χ}_{yx} extracted from (c) in polar coordinates. Compared with the case of $B \| xz$, it is significantly suppressed. (e) ρ_{xx} for $B \| xz$. (f) ρ^{χ}_{xx} obtained from (e). It is essentially zero except for the spikes at $\theta = \pm 90°$, which is an artifact due to the discontinuities. (g) ρ_{xx} for $B \| yz$. The asymmetry and the difference between two discontinuities are evidence. The resistivity value is different from that in (e) as two different electrodes were used due to failure of an electrode. (h) ρ^{χ}_{xx} obtained from (g) in polar coordinates, showing the same antisymmetry relations with ρ^{χ}_{yx}.

both the magnetic field and magnetization in a TRS broken Weyl semimetal $Co_3Sn_2S_2$. These effects originate from the interplay of the Berry curvature, the tilt of Weyl nodes and the chiral anomaly. Our work unveils an unusual property of magnetic Weyl semimetals and provides an example of antisymmetric linear magnetoresistance.

We are grateful for discussions with X. C. Xie, H. W. Liu, H. Jiang, and Q. H. Liu. This work was mainly supported by National Key Basic Research Program of China (No. 2016YFA0300600, No. 2020YFA0308800) and NSFC (Projects No. 11774009, No. 12074009). Z. L. Li acknowledges support from National Postdoctoral Program for Innovative Talents (Project No. BX201700012), Beijing Natural Science Foundation (Project No. Z200008) and the Youth Innovation Promotion Association of CAS (No. 2021008).

*lizhilin@iphy.ac.cn
†xswu@pku.edu.cn

[1] L. Onsager, Phys. Rev. **37**, 405 (1931).
[2] S. Liang, J. Lin, S. Kushwaha, J. Xing, N. Ni, R. J. Cava, and N. P. Ong, Phys. Rev. X **8**, 031002 (2018).
[3] A. A. Burkov, Phys. Rev. B **96**, 041110(R) (2017).
[4] S. Nandy, G. Sharma, A. Taraphder, and S. Tewari, Phys. Rev. Lett. **119**, 176804 (2017).
[5] N. Kumar, S. N. Guin, C. Felser, and C. Shekhar, Phys. Rev. B **98**, 041103(R) (2018).
[6] H. Li, H.-W. Wang, H. He, J. Wang, and S.-Q. Shen, Phys. Rev. B **97**, 201110(R) (2018).
[7] N. Nagaosa, J. Sinova, S. Onoda, A. H. MacDonald, and N. P. Ong, Rev. Mod. Phys. **82**, 1539 (2010).
[8] D. Xiao, M.-C. Chang, and Q. Niu, Rev. Mod. Phys. **82**, 1959 (2010).
[9] P. Jacquod, R. S. Whitney, J. Meair, and M. Büttiker, Phys. Rev. B **86**, 155118 (2012).
[10] Y. Wang, P. A. Lee, D. M. Silevitch, F. Gomez, S. E. Cooper, Y. Ren, J.-Q. Yan, D. Mandrus, T. F. Rosenbaum, and Y. Feng, Nat. Commun. **11**, 216 (2020).
[11] A. Cortijo, Phys. Rev. B **94**, 241105(R) (2016).
[12] V. A. Zyuzin, Phys. Rev. B **95**, 245128 (2017).
[13] G. Sharma, P. Goswami, and S. Tewari, Phys. Rev. B **96**, 045112 (2017).
[14] Y.-W. Wei, C.-K. Li, J. Qi, and J. Feng, Phys. Rev. B **97**, 205131 (2018).
[15] D. Ma, H. Jiang, H. Liu, and X. C. Xie, Phys. Rev. B **99**, 115121 (2019).
[16] K. Das and A. Agarwal, Phys. Rev. B **99**, 085405 (2019).
[17] A. Johansson, J. Henk, and I. Mertig, Phys. Rev. B **99**, 075114 (2019).
[18] A. Kundu, Z. B. Siu, H. Yang, and M. B. A. Jalil, New J. Phys. **22**, 083081 (2020).
[19] C. Xiao, H. Chen, Y. Gao, D. Xiao, A. H. MacDonald, and Q. Niu, Phys. Rev. B **101**, 201410(R) (2020).
[20] See Supplemental Material at http://link.aps.org/supplemental/10.1103/PhysRevLett.126.236601 for optical images of crystals, additional data, and theoretical analysis.
[21] E. Liu *et al.*, Nat. Phys. **14**, 1125 (2018).
[22] Q. Wang, Y. Xu, R. Lou, Z. Liu, M. Li, Y. Huang, D. Shen, H. Weng, S. Wang, and H. Lei, Nat. Commun. **9**, 3681 (2018).
[23] S. N. Guin, P. Vir, Y. Zhang, N. Kumar, S. J. Watzman, C. Fu, E. Liu, K. Manna, W. Schnelle, J. Gooth, C. Shekhar, Y. Sun, and C. Felser, Adv. Mater. **31**, 1806622 (2019).

[24] G. Li *et al.*, Sci. Adv. **5**, eaaw9867 (2019).
[25] D. F. Liu *et al.*, Science **365**, 1282 (2019).
[26] N. Morali, R. Batabyal, P. K. Nag, E. Liu, Q. Xu, Y. Sun, B. Yan, C. Felser, N. Avraham, and H. Beidenkopf, Science **365**, 1286 (2019).
[27] J.-X. Yin *et al.*, Nat. Phys. **15**, 443 (2019).
[28] Z. Guguchia *et al.*, Nat. Commun. **11**, 559 (2020).
[29] E. Lachman, R. A. Murphy, N. Maksimovic, R. Kealhofer, S. Haley, R. D. McDonald, J. R. Long, and J. G. Analytis, Nat. Commun. **11**, 560 (2020).
[30] J. Shen, Q. Yao, Q. Zeng, H. Sun, X. Xi, G. Wu, W. Wang, B. Shen, Q. Liu, and E. Liu, Phys. Rev. Lett. **125**, 086602 (2020).
[31] Y. Xu, J. Zhao, C. Yi, Q. Wang, Q. Yin, Y. Wang, X. Hu, L. Wang, E. Liu, G. Xu, L. Lu, A. A. Soluyanov, H. Lei, Y. Shi, J. Luo, and Z.-G. Chen, Nat. Commun. **11**, 3985 (2020).
[32] H. Yang, W. You, J. Wang, J. Huang, C. Xi, X. Xu, C. Cao, M. Tian, Z.-A. Xu, J. Dai, and Y. Li, Phys. Rev. Mater. **4**, 024202 (2020).
[33] R. Yang, T. Zhang, L. Zhou, Y. Dai, Z. Liao, H. Weng, and X. Qiu, Phys. Rev. Lett. **124**, 077403 (2020).
[34] S.-Y. Yang, J. Noky, J. Gayles, F. K. Dejene, Y. Sun, M. Dorr, Y. Skourski, C. Felser, M. N. Ali, E. Liu, and S. S. P. Parkin, Nano Lett. **20**, 7860 (2020).
[35] A. A. Burkov, Phys. Rev. Lett. **113**, 187202 (2014).
[36] J. Shen, Q. Zeng, S. Zhang, W. Tong, L. Ling, C. Xi, Z. Wang, E. Liu, W. Wang, G. Wu, and B. Shen, Appl. Phys. Lett. **115**, 212403 (2019).
[37] W. Schnelle, A. Leithe-Jasper, H. Rosner, F. M. Schappacher, R. Pöttgen, F. Pielnhofer, and R. Weihrich, Phys. Rev. B **88**, 144404 (2013).
[38] J. Xiong, S. K. Kushwaha, T. Liang, J. W. Krizan, M. Hirschberger, W. Wang, R. J. Cava, and N. P. Ong, Science **350**, 413 (2015).
[39] Q. Li, D. E. Kharzeev, C. Zhang, Y. Huang, I. Pletikosic, A. V. Fedorov, R. D. Zhong, J. A. Schneeloch, G. D. Gu, and T. Valla, Nat. Phys. **12**, 550 (2016).
[40] Z. Wang, Y. Sun, X.-Q. Chen, C. Franchini, G. Xu, H. Weng, X. Dai, and Z. Fang, Phys. Rev. B **85**, 195320 (2012).
[41] The detail of the experimental observations and their implication will be reported elsewhere.